sustainability

MDPI

Article

Enhanced Adaptive Dynamic Surface Sliding Mode Control for Optimal Performance of Grid-Connected Photovoltaic Systems

Hashim Alnami [1], Sultan H. Hakmi [1], Saad A. Mohamed Abdelwahab [2,*], Walid S. E. Abdellatif [2], Hossam Youssef Hegazy [3], Wael I. Mohamed [3] and Moayed Mohamed [4]

[1] Department of Electrical and Electronic Engineering, College of Engineering and Computer Science, Jazan University, P.O. Box 114, Jazan 45142, Saudi Arabia; halnami@jazanu.edu.sa (H.A.); shhakmi@jazanu.edu.sa (S.H.H.)
[2] Electrical Department, Faculty of Technology and Education, Suez University, Suez 43221, Egypt; walid.abdellatif@ind.suezuni.edu.eg
[3] Electrical Department, Faculty of Technology and Education, Helwan University, Helwan 11795, Egypt; hossamyh@hotmail.com (H.Y.H.); waelibrahim785@gmail.com (W.I.M.)
[4] Electrical Department, Faculty of Technology and Education, Sohag University, Sohag 82524, Egypt; moayed1190@techedu.sohag.edu.eg or moayedm1990@gmail.com
* Correspondence: saad.abdelwahab@suezuniv.edu.eg

Abstract: This study presents an enhanced, adaptive, and dynamic surface sliding mode control (SMC), a cutting-edge method for improving grid-connected photovoltaic (PV) system performance. The suggested control approach uses dynamic SMC and adaptive approaches to enhance the robustness and efficiency of a system. Proportional–integral (PI) and SMC, two control systems for maximum power point tracking (MPPT) in PV systems, are compared in this paper. This study finds that the SMC system is a more effective and efficient MPPT approach for PV systems compared to the conventional PI control system. The SMC system's unique feature is the capacity to stabilize grid voltage and attain a modulation index of less than one. An important component of power electronic system control is the index, which acts as a parameter representing the relationship between the output signal's amplitude and the reference signal's amplitude. The SMC method demonstrates improved robustness, efficiency, and stability, especially in dynamic operating settings with load and solar radiation changes. Compared to the PI control, the SMC exhibits a noteworthy 75% reduction in voltage fluctuations and an improvement in the power output of 5% to 10%. Regarding output power optimization, voltage stability, and accurate current tracking, the SMC system performs better than the PI control system. Furthermore, the SMC technique maintains a modulation index below one and guarantees grid voltage stability, both of which are essential for the efficiency and stability of power electrical systems.

Keywords: PV system; MPPT; PI control; SMC

Citation: Alnami, H.; Hakmi, S.H.; Abdelwahab, S.A.M.; Abdellatif, W.S.E.; Hegazy, H.Y.; Mohamed, W.I.; Mohamed, M. Enhanced Adaptive Dynamic Surface Sliding Mode Control for Optimal Performance of Grid-Connected Photovoltaic Systems. *Sustainability* **2024**, *16*, 5590. https://doi.org/10.3390/su16135590

Academic Editor: Marc A. Rosen

Received: 7 March 2024
Revised: 8 June 2024
Accepted: 27 June 2024
Published: 29 June 2024

1. Introduction

Dynamic power transactions, varying electricity pricing, and the intermittent nature of renewable energy output in relation to load demand are some of the issues grid-connected PV systems face [1]. The PV system and the grid must be seamlessly integrated to harvest generated power efficiently. The PV system and the electricity grid's utility must meet technical requirements to guarantee safety and dependability. Grid-connected solar sources usually use DC–AC inverters to supply P and/or Q to the line. Appropriate power control strategies are required for inverters to manage the amount of P and Q injection to meet the local load profile. Several power electronics-based techniques, such as the widely used vector-type control, have been developed to regulate P and Q injection. Furthermore, PV arrays can produce the required amount of Q with proper inverter controls to provide voltage support [2,3].

In [2], the authors examined hybrid renewable hydrogen systems intended for stand-alone use. They achieved this by modeling hybrid PV-H2 systems through simulations. This strategy combined PV technology, which turns sunshine into electricity, with renewable energy-powered hydrogen (H2) manufacturing devices. The study assessed the effectiveness, viability, and possible advantages of combining these technologies to produce self-sufficient and sustainable energy solutions using simulations. Fuel cells use electrochemical reactions to make electricity, whereas PV panels use sunshine to generate power. Moreover, Yunez-Cano et al. investigated a PV/H2 system, including measurements of the H2 unit's dimensions and assessments of the power production of the solar array [4]. Most research has concentrated on using PV energy as a stand-alone or grid-connected system with storage options. However, little research has been conducted on integrating PV interconnections with hydrogen fuel systems. It faces multiple challenges, including fluctuating electricity prices, power transaction momentum, and the disparity between renewable energy production and load demand [4].

The PID controller's performance and the hybrid renewable energy system's overall stability and efficiency were improved by [5]. It used the ASCA technique to dynamically modify the PID controller's gains to maximize its adaptability to changing circumstances and variations in load. This enhanced the system's capacity to sustain precise and steady control under various operational conditions. The study intended to increase disturbance rejection, minimize transient responses, and improve reference signal tracking by optimizing the PID controller using AS-CA-based methods, ultimately improving system performance.

In [6], a novel method for controlling voltage in distribution networks was presented, which tackles the difficulties caused by random PV power generation. The project aimed to improve voltage stability, reduce infrastructure costs, and facilitate the effective integration of renewable energy sources into distribution networks by employing a hierarchical control technique and accounting for PV production unpredictability.

Presenting a novel converter-less control technique for a hybrid renewable energy system that combines fuel cells, solar PV, wind, and battery energy storage was the aim of [7]. The goal of [8] was to do away with traditional power electronic converters, which would simplify the architecture and improve the system's overall performance, stability, and efficiency. Offering a novel strategy for enhancing the performance of hybrid energy systems advanced the fields of control techniques and renewable energy systems.

Three-phase PV grid-connected inverters working in unbalanced grid situations were the subject of a comparative examination of current control techniques in [9]. For grid-connected PV systems, the research offered useful insights into controlling current imbalances and preserving system stability by assessing the effectiveness of various control mechanisms.

The plan reduced harmonics, improved performance in low-voltage situations, and synchronized the grid without needing a phase-locked loop (PLL) in unusual grid scenarios [10]. Instead of depending on traditional PLL approaches, it used cutting-edge techniques to accomplish grid synchronization, guarantee continuous operation during voltage decreases, and increase power quality. By offering a creative control approach that improved the efficiency and stability of grid-connected solar systems, it advanced the fields of power electronics and renewable energy systems [10].

The creation of a control plan for PV-STATCOM, a hybrid PV and synchronous condenser system had the efficient control of reactive power and grid voltage as the primary goals. The method used a cutting-edge idea known as the Synchronverter, which combines a synchronous machine with a power electronic converter to improve grid stability and power quality. This creative approach advanced grid support technology and power electronics applications for integrating renewable energy [11].

In our study, we extensively analyzed the performance of both the SMC and traditional PI control systems in the context of MPPT for PV systems. Our evaluation encompassed various operational scenarios, including dynamic changes in solar radiation and load conditions.

This study's key contribution and validity lie in improving the performance of PV systems connected to a grid. It was made possible by a suggested strategy that increases system efficiency and robustness by utilizing SMC and adaptive approaches. PI control and SMC, two control schemes for MPPT in PV systems, are compared in this paper. Both control systems' performance were assessed under various operational scenarios, including load and solar radiation variations. According to this investigation, under rapidly changing weather and solar radiation conditions, the SMC system performed better than the PI control system regarding voltage stability, current tracking, and output capability. Adaptive methods were used to increase the system's resilience and efficiency, enabling it to change in response to environmental conditions. As a result, the system achieved high performance and stability even amidst load fluctuations and solar radiation variability, highlighting the clear superiority of the SMC system compared to the PI control system.

This strategy employs innovative techniques to improve power quality, such as reducing voltage fluctuations and minimizing harmonic distortions. It contributes to the stability and reliability of the electrical grid.

This technique guarantees continued functioning during voltage drops, which can harm system performance for various reasons. By keeping the solar system operating smoothly even in the event of voltage decreases, this technique upholds the dependability of the power supply.

Summarizing the research introduction, Table 1 presents a comparative analysis of the approaches that have been applied in various studies on renewable and non-renewable energy systems. It is possible to gain a better knowledge of the evolution and trends in this field over time by contrasting the characteristics of the current study with those of earlier studies. It is also useful for determining gaps in the state of the field and assessing the efficacy of various control strategies.

Table 1. Comparing the current study to previous research findings.

Reference	Year	Type of Renewable Energy	Technique Type
[1]	2021	Grid-connected PV system	PI and H-infinity Control (H∞C)
[2]	2013	Hybrid PV/fuel cell/battery/wind	PI control
[3]	2009	Hybrid PV/fuel cell/hydrogen tank	Conventional
[4]	2016	Hybrid PV/hydrogen (PV/H_2)	Conventional
[5]	2020	PV/wind and external battery charging	Sine cosine algorithm (SCA) and adaptive sine cosine optimization algorithm (ASCA)
[8]	2019	Conventional	Control method for Z-axis MEMS gyroscopes using fractional calculus and adaptive dynamic S.M.C. method
[12]	2020	Conventional	ASTNLFOPIDSMC
[13]	2015	Conventional	NTSMC and NFTSMC
[14]	2019	Conventional	NFTSM and NN algorithm
[15]	2004	Conventional	Artificial neural network
[16]	2013	PV and diesel generator	Conventional
[6]	2023	PV system	Admissible range (AR) and affine decision rule (ADR)
[7]	2023	Hybrid PV/wind/fuel-cell system, with battery energy storage	Artificial intelligence-based algorithm
[9]	2023	Grid-connected PV system	Average active–reactive control (AARC) and fuzzy logic
[10]	2023	Grid-connected PV system	Multiobjective control strategy (MOCS) and conventional control strategy (COCS)
[11]	2023	Grid-connected PV system	Active–reactive control by microcontroller
Case study	___	Grid-connected PV systems	PI and adaptive dynamic sliding mode control

This study aims to examine and contrast the use of two control strategies, PI and SMC, in a grid-connected PV system that operates in different solar radiation scenarios. This study

looks into how the system reacts to variations in solar radiation, which greatly impact the PV array's power output. Various performance metrics, such as tracking accuracy, steady-state error, and resilience to disturbances, are employed to evaluate and contrast the effectiveness of the two control strategies. The findings of this study provide valuable insights into the feasibility and efficiency of employing these control strategies within grid-connected PV systems, especially when faced with changing solar radiation levels.

2. System Description

Figure 1 shows the schematic of a three-phase grid-connected PV generating system. It is composed of two main parts: the control part, which integrates MPPT, PI, and SMC into an inverter controller for the three-phase PV grid-connected system; and the power part, which includes a PV array source, DC link capacitor, converter, inverter, RL filter, transformer, and grid connection.

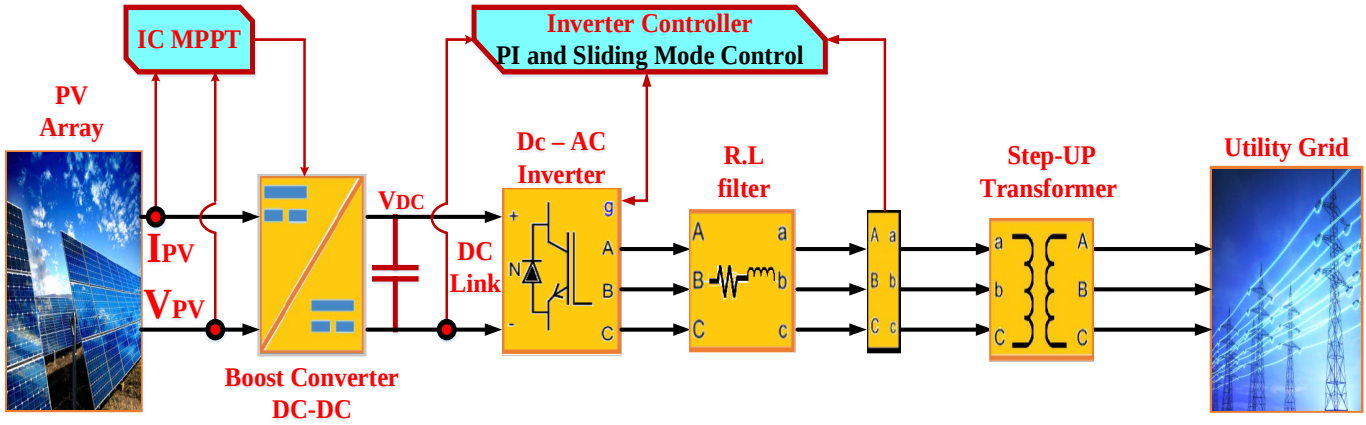

Figure 1. Grid-connected simulation modeling of the PV system using PI and SMC.

This study's controller uses a variable step-size approach to increase system responsiveness. The P-V curve is compared with a freshly created curve to find the ideal step size, locating the operational point either close to the MPPT region or on a distant P-V characteristic. If the operating point is distant from the MPPT, the controller applies a high voltage reference equivalent to the step voltage.

2.1. Proposed Control of the Three-Phase Grid-Connected System

The PV power generation system's efficient use of generated power is one of its main benefits when connected to a grid [17–20]. The crucial phase of the mathematical modeling for PV cells, which is a basic component of the analysis and design of PV control systems, is shown in Figure 2. The equation shows the temperature and PV current relationship, affecting the PV array's energy output.

$$I = I_{Ph} - I_0\left[e^{\frac{q(V+IR_S)}{AKT_C}} - 1\right] - \frac{V + IR_s}{R_{Sh}} \quad (1)$$

where I is the PV current of the PV module, I_0 is the saturation current of the diode, I_{Ph} is the generated current from the PV system, R_S is the resistance of series in Ω, R_{Sh} is the resistance of parallel in Ω, K is the constant of Boltzmann, q is the charge of the electron, and T is the temperature [°K].

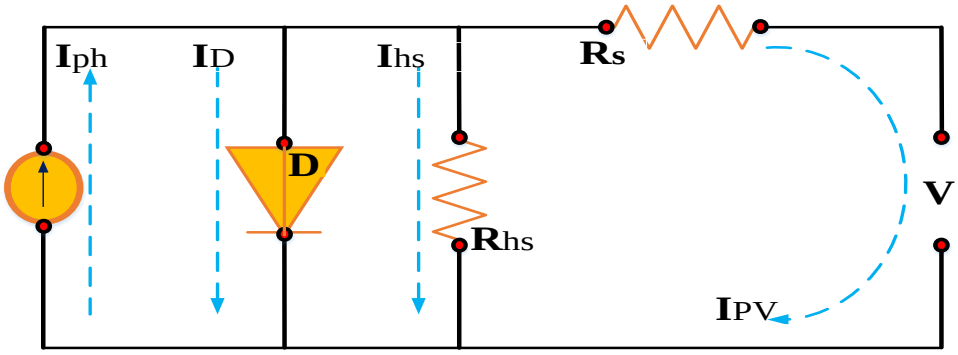

Figure 2. PV cell equivalent circuit.

The inverter is essential for connecting PV systems to a grid by converting DC power to AC. As shown in Figure 3, the controller system used in this study uses a four-step procedure. It first subjects the system to Park's transformations. The controller system then goes through four stages, as shown in Figure 3. To ensure operation at the unity power factor, the reference currents (Iqref and Idref) are first compared with the actual currents (Iq and Id). It then compares the VSI output voltage signal with the reference voltage signal to generate the PWM signals, modifying the inverter's switching sequence to control the output voltage and current [4,21–27]. Grid-connected PV systems can operate efficiently in various solar radiation scenarios thanks to this all-inclusive control system. To further detect the grid frequency and produce the angle (θ) needed to synchronize the inverter with the grid, a phase-locked loop (PLL) is employed. By employing Park's transformations, this angle makes it easier to convert the reference currents from stationary to revolving reference frame values, which are then compared with the actual currents. To guarantee that the inverter sends power to the main grid at the proper voltage, frequency, and power factor, the current regulators' error signals are used as the inputs.

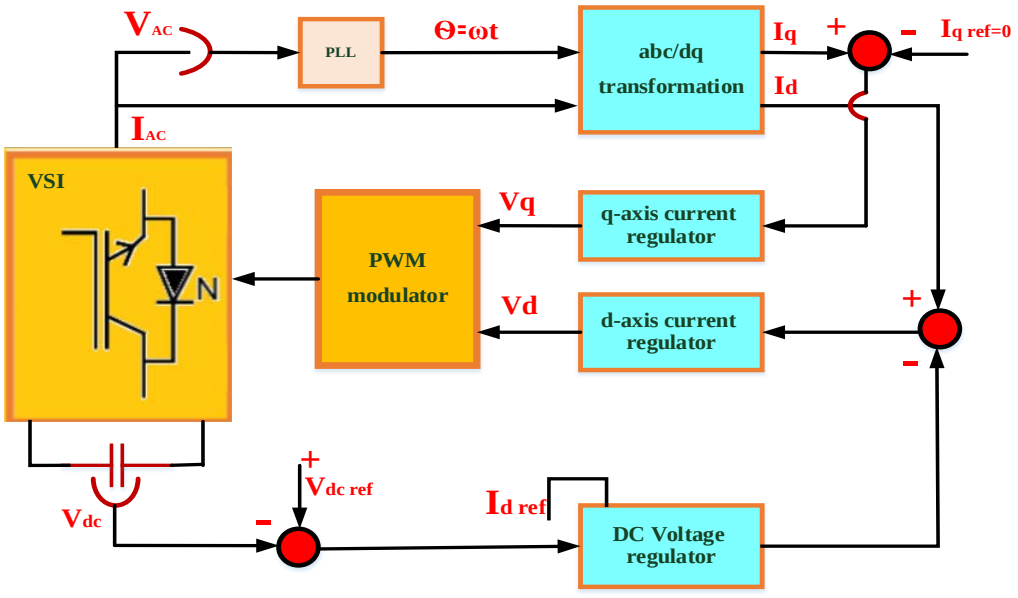

Figure 3. Block diagram of the controller for the inverter of a system.

The PWM approach manages the switches and the inverter's output voltage and current by producing switching signals at a set frequency and adjusting the duty cycle. To guarantee effective power transfer to the grid, the VSI is operated at unity power factor. The controller ensures power quality and system stability, which regulates the VSI's output

voltage and current to maintain a consistent voltage and frequency at the point of common coupling (PCC) with the grid [27].

To obtain the currents flowing from the VSI to the grid, a synchronous d-q axes transformation is used, which is expressed by the following equations [27]:

$$I_d = \int \frac{1}{L_{(A,B,C)}} \left(V_{0d} - R_{(A,B,C)} I_d + L_{(A,B,C)} \omega_S I_q - V_{(A,B,C)q} \right) \quad (2)$$

$$I_q = \int \frac{1}{L_{(A,B,C)}} \left(V_{0q} - R_{(A,B,C)} I_q + L_{(A,B,C)} \omega_S I_d - V_{(A,B,C)q} \right) \quad (3)$$

$$P_{inv} = V_{od} I_d + V_{oq} I_q \quad (4)$$

$$Q_{inv} = V_{oq} I_d + V_{od} I_q \quad (5)$$

where P_{inv}, Q_{inv} are the active and reactive power outputs from the VSI to the grid; $I_{d,}$ I_q are the currents flowing from the VSI to the grid in the d-q axis; V_{0d}, V_{0q} are the phase voltages in the d-q axis; ω_S is the desired angular velocity command; $V_{(A,B,C)q}$, $V_{(A,B,C)q}$ are the phase voltages a, b, and c from the VSI to the grid in the d-q axis; $R_{(A,B,C)}$ is a symmetrically configured three-phase resistor; and $L_{(A,B,C)}$ is the inductor impedance.

2.2. PI Control

Utilizing a PI controller, the dynamic total error signals are addressed. The controller's objective is to reduce the dynamic total error signal to zero as the system comes closer to the intended operation state. The PI controller controls the output voltage, which operates based on the error between the reference and output signals. An output proportionate to the instantaneous error is produced by the proportional control component, and an output proportional to the integral of the error is produced by the integral control component. The block diagram of the PI controller is shown in Figure 4. A standard PI controller's transfer function can be written as follows [26–31]:

$$G_s(s) = K_p + K_I/s \quad (6)$$

where K_P, K_I is the PI controller gains for proportional and integral control gain and $G_s(S)$ is the function of the variable s.

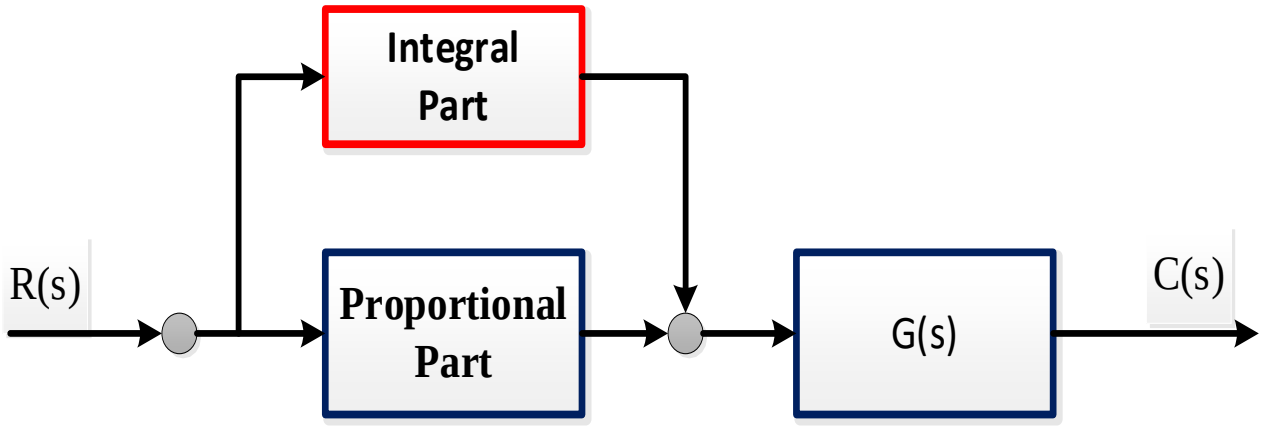

Figure 4. PI controller block diagram.

2.3. Adaptive Surface SMC

SMC is a technique used in systems with variable structures. This method, characterized by its discontinuous nature, attains control by employing certain control inputs to move the operational point of the system along a manifold or sliding surface. Choosing an appropriate sliding surface is part of the controller's design process. SMC is an adap-

tive control method that amplifies the controller's proportional gain, improving system accuracy and reactivity [24–26].

SMC is shown graphically in Figure 5 utilizing a phase plane depiction. The error (e(t)) and its derivative ($\dot{e}$(t)) are included in this representation. It is observed that, independent of the initial conditions, the trajectory of the system converges to the surface in a finite amount of time (the reaching mode), and then moves along the surface in the direction of the desired destination (the sliding mode) [31–35]. Making a custom sliding surface is the first step of the SMC design process. The system's dynamics are confined to this sliding surface to follow the equations of the surface, guaranteeing stability and alignment with the intended parameters.

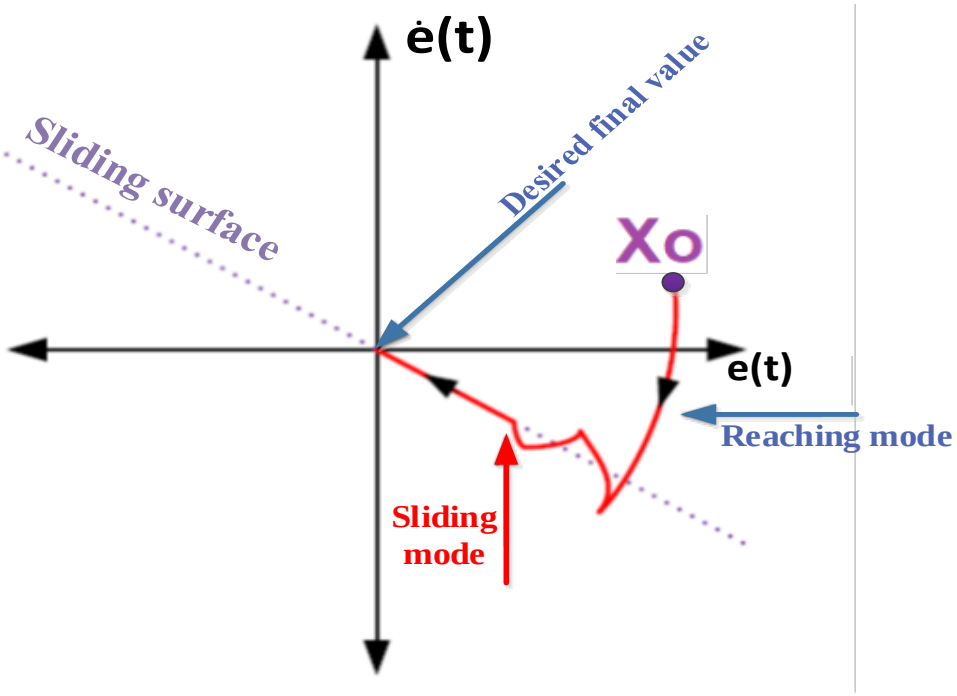

Figure 5. SMC form interpretation.

Creating a feedback control law that allows the system's trajectory to approach the sliding surface is essential to achieving the sliding surface in time. The sliding mode refers to how the system moves on the sliding surface. Notably, the tracking error, e(t), and its derivatives influence the sliding surface, denoted as S(t) [34,35].

$$S(t) = \left(\lambda + \frac{d}{dt}\right)^{n-1} e(t) \tag{7}$$

where n denotes the system order and λ is a positive scalar that shapes S(t). The designer selects λ and plays a crucial role in determining the system's performance on the sliding surface [34,35]. Specifically, for a second-order process (when n = 2), the first-time derivative of the sliding surface, as indicated by Equation (7), is expressed as follows:

$$\dot{S}(t) = \lambda\dot{e}(t) + \ddot{e}(t), \ldots \tag{8}$$

The standard approach for deriving the corresponding SMC legislation is Filippov's construction. The primary goal of control is to guarantee that the controlled variable reaches the reference value. This means that in a steady state, the tracking error e(t)

and its derivatives have to approach zero. The following procedural actions are taken to accomplish this goal:

$$\frac{d\mathrm{S}(t)}{dt} = \dot{S}(t) = 0 \tag{9}$$

Formulating a control law that ensures the controlled variable converges towards its reference value while complying with Equation (9) comes after the sliding surface has been chosen. This control law can be derived by changing the selected sliding surface in the system's dynamic equations. The SMC law, denoted as U_{SMC}(t), typically achieves rapid motion to bring the system state onto the sliding surface followed by slower motion.

The SMC law comprises two additive components: a continuous segment, U_C(t), and a discontinuous segment, U_d(t).

$$U_{\mathrm{SMC}}(t) = U_C(t) + U_d(t) \tag{10}$$

When examining the tracking error, denoted as e(t), which represents the difference between the reference signal r(t) and the system output y(t), a sliding surface in the error space can be defined using the coefficients obtained for the control law. This control law is recognized as the predictive PID control law. The sliding surface can be articulated as follows:

$$S(t) = K_P e(t) + K_I \int_0^t e(t)dt + K_D \frac{de(t)}{dt} \tag{11}$$

where $\mathrm{K_P}$, $\mathrm{K_I}$, $\mathrm{K_D}$ are the design parameters.

If the initial error at time t = 0 is e(0) = 0, the tracking objective can be conceptualized as maintaining the error on the sliding surface S(t) = 0 for all $\mathrm{t} \geq 0$. Once the system trajectory reaches the sliding surface S(t) = 0, it persists on it while sliding toward the origin, $\mathrm{e}(t) = 0$ and $\dot{\mathrm{e}}(t) = 0$.

An SMC law's primary goal is to direct the error e(t) in the direction of the sliding surface, and then follow it as it moves in the direction of the origin. Because of this, the sliding surface's stability is critical, which means that:

$$\lim_{t \to \infty} e(t) = 0 \tag{12}$$

The control goal is to ascertain a control input u(t) in such a manner that the closed-loop system adeptly traces the intended trajectory, implying that the tracking error e(t) should converge to zero. The SMC process can be delineated into two distinct phases:

Sliding Phase (S(t) = 0): During this phase, the system operates in a manner where the sliding surface S(t) remains at zero and its derivative $\dot{S}(t)$ also remains zero.

Reaching Phase ($\mathrm{S(t)} \neq 0$): In this phase, the system deviates from the sliding surface S(t), and S(t) becomes nonzero.

These two phases, which are each independently derived, correlate to two different sorts of control laws:

- Sliding Control: This control law is used when the system is nearing S(t) = 0 or in the sliding phase. Maintaining the system on the sliding surface is its main goal.
- Hitting Control: This control law is triggered when the system is in the reaching phase, or when S(t) is not equal to zero. Its purpose is to direct the system towards the sliding surface once again.

These two control laws collaborate to ensure that the system reaches the sliding surface and remains on it to achieve the desired tracking performance. The derivative of the sliding surface defined by Equation (11) can be expressed as

$$\dot{S}(t) = K_P \dot{e}(t) + K_I e(t) + K_D \ddot{e}(t) \tag{13}$$

An essential requirement for the output trajectory to stay on the sliding surface S(t) is that $\dot{S}(0) = 0$.

$$K_P\dot{e}(t)\ \ K_I e(t) + K_D\ddot{e}(t)\ \ = 0 \tag{14}$$

If the control gains K_p, K_I, and K_D are accurately chosen with proper consideration of the prediction horizon, control horizon, and weights, and ensuring that the characteristic polynomial is strictly Hurwitzian—indicating that the roots of the polynomial are strictly located in the open left half of the complex plane—this suggests that:

$$\lim_{t\to\infty} e(t) = 0 \tag{15}$$

The discrepancy, e(t) = r(t) − y(t), can be expressed concerning the physical parameters of the plant, with r(t) representing the command signal and y(t) signifying the measured output signal. The discontinuous segment of SMC, identified as U_d(t), commonly incorporates a nonlinear element encompassing the control law's switching element. This controller aspect is recognized for its discontinuity precisely at the sliding surface. It is frequently structured based on a relay-like function, allowing for swift transitions between control structures with a theoretically infinite switching speed.

The successive stages involved in fine-tuning the SMC system, as outlined by Equation (7) through (15), are illustrated visually in the flow chart presented in Figure 6. This diagram provides an organized synopsis of the tuning procedure, detailing each stage and their interrelationships to attain efficient control.

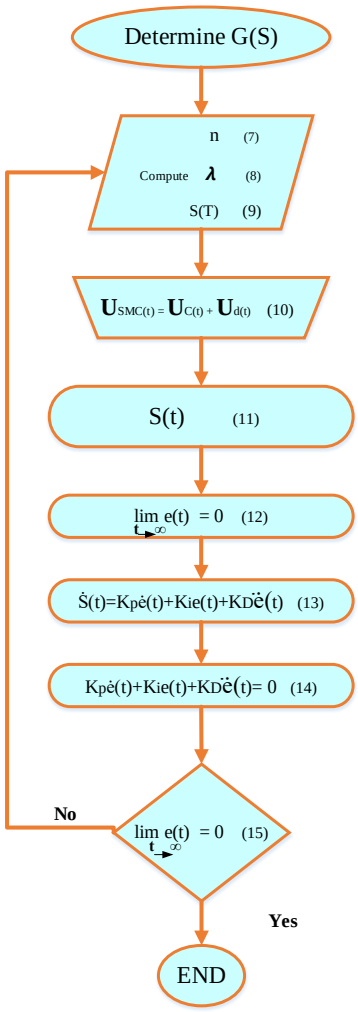

Figure 6. Flow chart for SMC tuning.

3. Results and Discussion Comparison of Simulation for PI Control System and SMC

3.1. Comparison Results under Ramp Changes in Solar Radiation

Table 2 contains the specifics on the system. A comparison of the PV's maximum power output under different solar radiation conditions utilizing two alternative control schemes—PI and SMC—is shown in Figure 7. The PV current and variations in radiation are tightly correlated, as Figure 7A illustrates. The current fluctuates slightly between 0 and 0.5 s at a temperature of 25 °C and a radiation intensity of 330 W/m^2. Subsequently, the radiation starts to increase, reaching 660 W/m^2 between 0.5 and 1 s. The current is 480 A, and the radiation stabilizes at 660 W/m^2 between 1 and 1.5 s. Then, between 1.5 and 2 s, the radiation drops to 260 W/m^2, which causes the current to drop. Starting between two and five seconds into the stabilization phase, the current is 190 A, somewhat less in the SMC than PI. From 2.5 to 3 s, the radiation begins to rise once more; from 3 to 3.5 s, it steadies at 470 W/m^2, and the current climbs from 350 to 380 A.

Table 2. PV system simulation specifications.

Parameters	Values
Maximum power of PV module	305.2 W
Short-circuit current of PV module	5.96 A
Open-circuit voltage of PV module	64.2 V
Maximum current of PV module	5.58 A
Maximum voltage of module	54.7 V
Parallel strings of PV array	132
Series-connected modules per string	5
Boost converter inductance	5 mH
Boost converter resistance	0.005 Ω
Boost converter capacitance	100 μF
Reference voltage of DC link	500 V
Filter inductance	0.25 mH
Filter resistance	0.015 Ω
Step-up transformer	260 V/25 kV
Voltage of grid	25 kV
Frequency of grid	60 Hz
K_p, current regulatory control at PI	0.5
K_i, current regulatory control at PI	25
K_p, voltage source control at PI	9
K_i, voltage source control at PI	950

The performance of PV systems using the SMC approach is shown in Figure 7B under different solar radiation circumstances. The PI control approach yields the maximum power output when the solar radiation rises from 330 W/m^2 to 660 W/m^2 within 0.5 and 1 s. Nevertheless, the power output stabilizes between 1 and 1.5 s, and the power outputs of the two approaches are the same. When it comes to maximizing PV energy extraction when solar radiation starts to decline, the SMC method outperforms the PI control method. The SMC method's power output does not change when radiation levels drop.

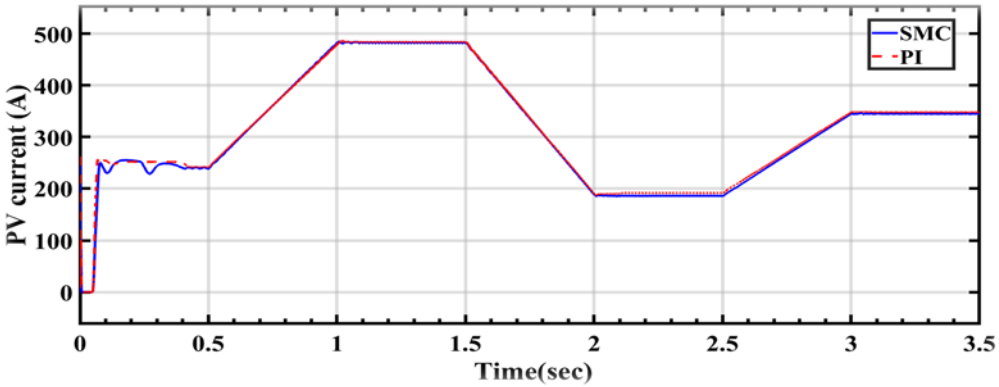

(**A**)

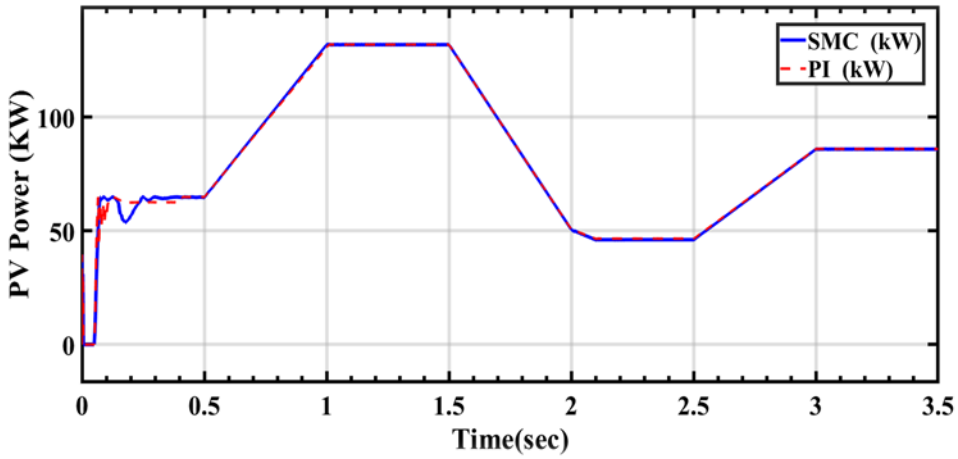

(**B**)

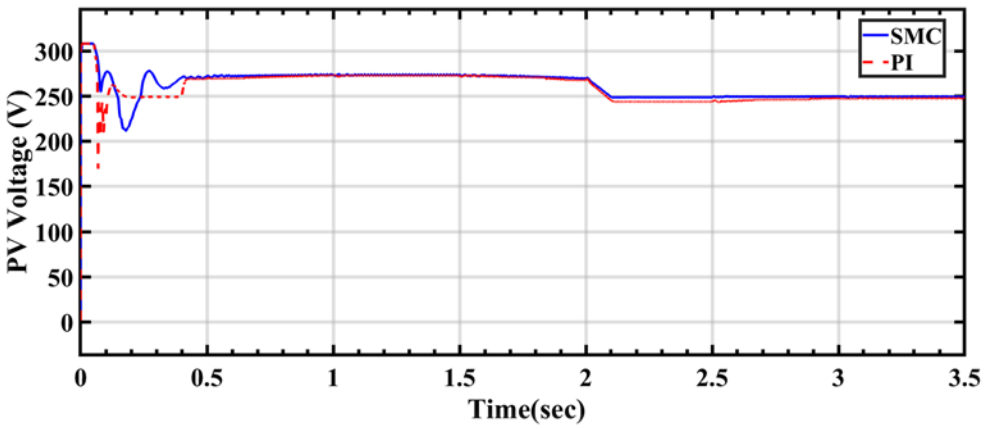

(**C**)

Figure 7. DC results for PV cell using a control system (SMC and PI) under ramp change irradiance. (**A**) Output of PV current, (**B**) output of PV power, and (**C**) output of PV voltage.

The voltage change in PV cells when utilizing SMC and PI as the two control methods is depicted in Figure 7C. While there is some initial oscillation in the voltage, the SMC method yields a more consistent voltage than the PI method. At 25 °C, a voltage of 280 V is stabilized in 0.5 s for both approaches; however, the SMC method exhibits a more stable and higher voltage than the PI method. The SMC approach has a larger voltage drop when the temperature reaches 50 °C at 2 s, but the PI method has a smaller voltage drop and

stabilizes at less than 250 V at 3.5 s. The voltage curve indicates that, in comparison to the PI approach, the SMC method maximizes the voltage of the PV cells.

The relationship between sun radiation levels (from 0 to 1 PU) and the d-axis current component is shown in Figure 8, where the q-axis current component is always zero. Every radiation level is shown on the graph to show that the d-axis current (Id) stays constant. The q-axis current component (Iq) also stays constant at zero for the same radiation levels. Remarkably, for every radiation level, the real Id value coincides with the reference current value for Idref. But Iqref's reference current value fluctuates at the same radiation levels, and Iq never goes below zero. In addition, when the SMC is used instead of the PI control, the system responds more quickly.

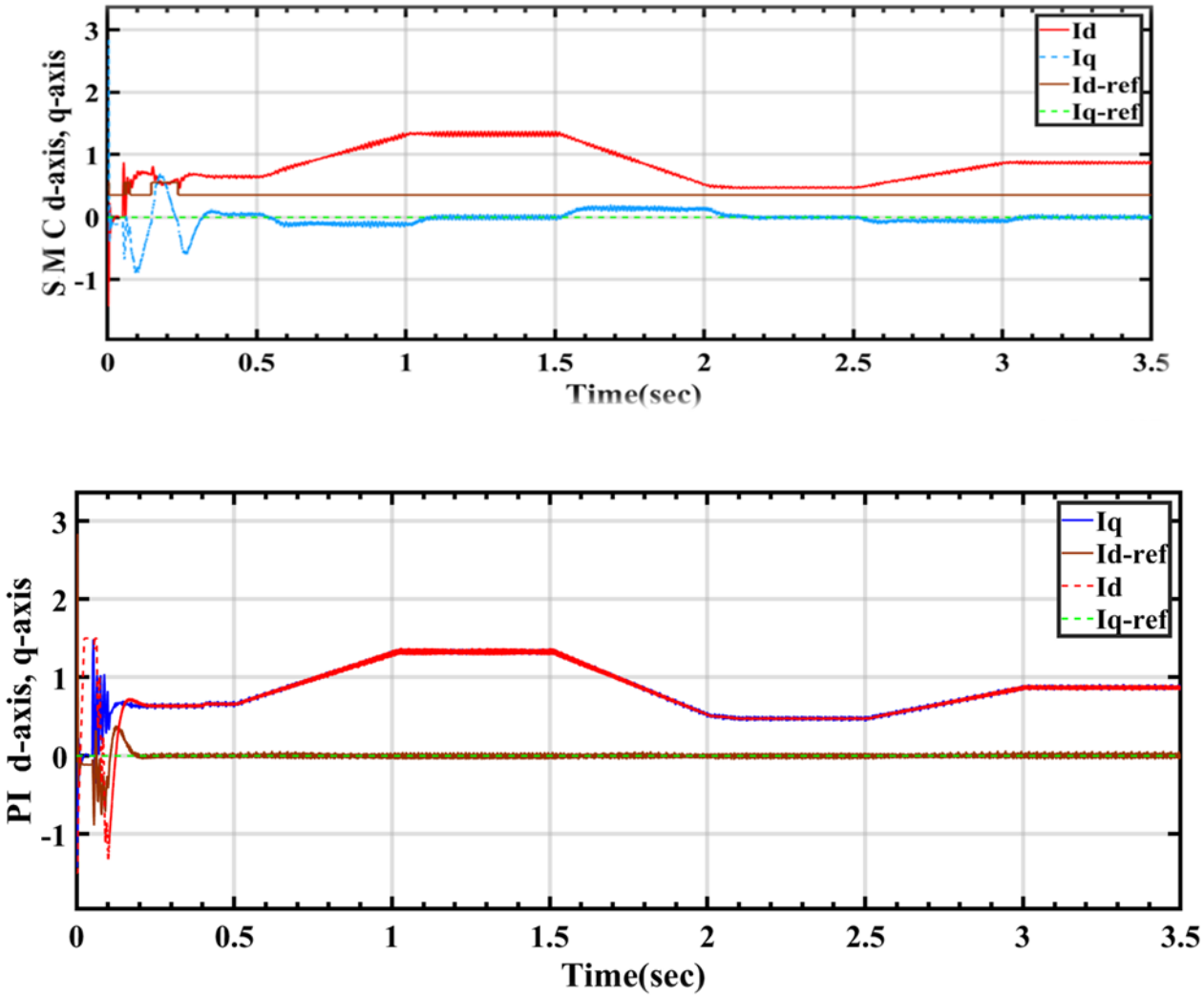

Figure 8. d-axis and q-axis currents under ramp change irradiance.

Figure 9 displays the SMC and PI control systems' active power (P) response to varying solar radiation over time. Both systems produce more active power when the amount of solar radiation rises. In contrast to the PI system, the SMC system appears to produce more energy, suggesting that the SMC system is more efficient at making use of the PV system.

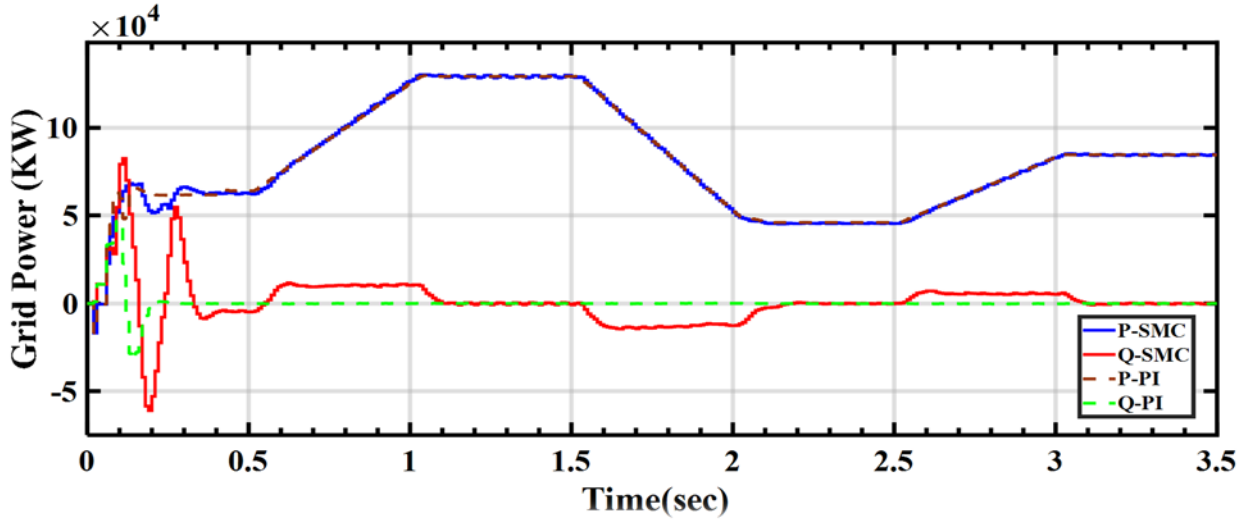

Figure 9. Grid active and reactive power under ramp change irradiance.

In Table 3, two distinct control methods, PI control and SMC, are used to compare how well a PV energy system performs. The data for different time intervals and solar irradiance levels are shown in the table. Varying irradiance levels and time intervals are noticeable in the voltage and power output under the PI control. Specifically, for 330 W/m^2 of irradiance and a 0 to 0.5 s time interval, the voltage varies between 248.933 V and 263.664 V, yielding power outputs of 63.876 kW and 62.5715 kW. Comparable variations are seen at various irradiance levels and time intervals under the PI control. In comparison, output voltage and power values are recorded as more steady when using the SMC. For instance, with 330 W/m^2 of irradiance and a time interval of 0 to 0.5 s, the voltage stays reasonably constant between 258.536 V and 271.457 V, yielding 64.858 kW and 64.885 kW of power output, respectively. This trend toward a more steady performance under SMC management is constant over a range of irradiance levels and time periods. The data indicate that, in comparison to the PI control, the SMC produces a more stable and consistent performance of the PV energy system, as seen by the lower levels of output voltage and power variations. This suggests that the implementation of an SMC could have benefits for preserving stable operation and maximizing energy production under different environmental circumstances.

As seen in Figure 10A, the grid voltage stability is indicated by the voltage component V_d for both the PI control and SMC methods, being near to 1 PU. Furthermore, Vq is close to zero for both approaches, indicating high efficiency. The modulation index for both systems is near to 1 PU, as shown in Figure 10B, further demonstrating their efficacy in preserving grid voltage stability and efficiency. The modulation index must be $\leq$1 for stability.

A comparison of grid-connected system performance under ramp variations in solar radiation under the two control schemes, PI and SMC, is shown in Table 4. The data for several time intervals are provided in the table. The grid power production under PI management fluctuates between 46.385 kW and 129.352 kW over the different time intervals. The current magnitude and phase angle variations are seen in the grid current fluctuations.

Table 3. Comparison of PV energy performance with PI and SMC under ramp changes in solar radiation.

Type of Controller	Irradiance (W/m^2)	Time (s)	V_{PV} (V)	P_{PV} (KW)
PI	330	0:0.5	248.933 (fluctuations)	62.5715
			263.664 (fluctuations)	63.876
	660	1:1.5	272.236 (fluctuations)	131.828
			272.223 (fluctuations)	131.865
	260	2:2.5	255.248 (fluctuations)	48.596
			243.699 (fluctuations)	46.579
SMC	330	0:0.5	258.536	64.858
			271.457	64.885
	660	1:1.5	274.112	131.928
			274.442	131.938
	260	2:2.5	259.013	48.5259
			248.436	46.1036

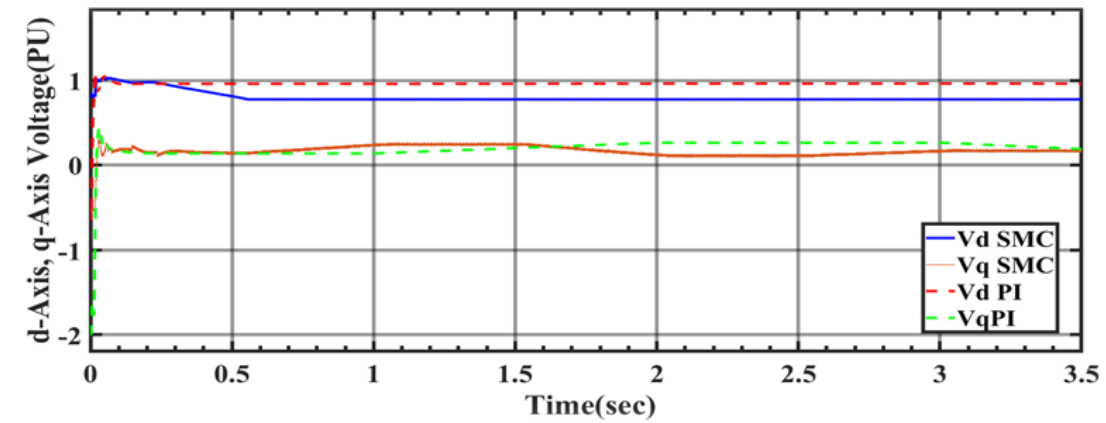

(**A**)

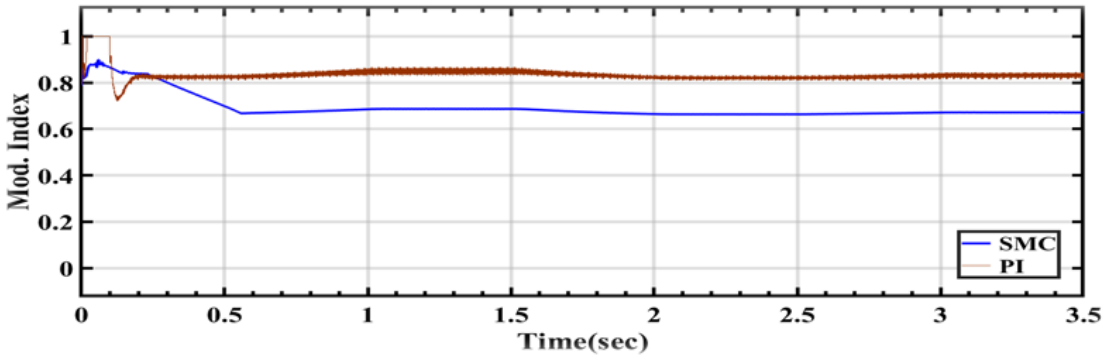

(**B**)

Figure 10. (**A**) d-axis and q-axis voltage (PU) and (**B**) modulation index.

Table 4. Comparison of grid performance results for PI and SMC under ramp changes in solar radiation.

Type of Controller	Time (s)	Grid Power (kW)	Grid I_d	Grid I_q
PI	0.1504	61.8671	0.8241	0.8425
	0.5033	62.5225	0.7362	0.7452
	1.2496	129.3521	1.4573	1.4624
	1.9898	53.580	0.5623	0.8524
	2.525	46.385	0.5321	0.5741
	3.221	84.558	0.8624	0.8741
SMC	0.1504	67.442	−0.5231	0.5426
	0.5033	66.039	0.03312	0.5624
	1.2496	129.960	0.01426	1.4328
	1.9898	55244.3	0.25425	0.9465
	2.525	46481.1	0.01542	0.6482
	3.221	84773.4	0.01454	0.8745

On the other hand, the SMC keeps the grid power output reasonably constant over the various time intervals, ranging from 46.481 kW to 129.960 kW. SMC-managed grid currents show very little variation in Grid Id and Grid Iq.

Figure 11 tracks the highest power point that may be connected to the grid by showing the link between the three-phase current and variation in radiation. Figure 11A shows the current change as it passes through the SMC system, and Figure 11B shows it as it passes through the PI control system. The SMC system is assumed to have a more steady beginning than the PI control system.

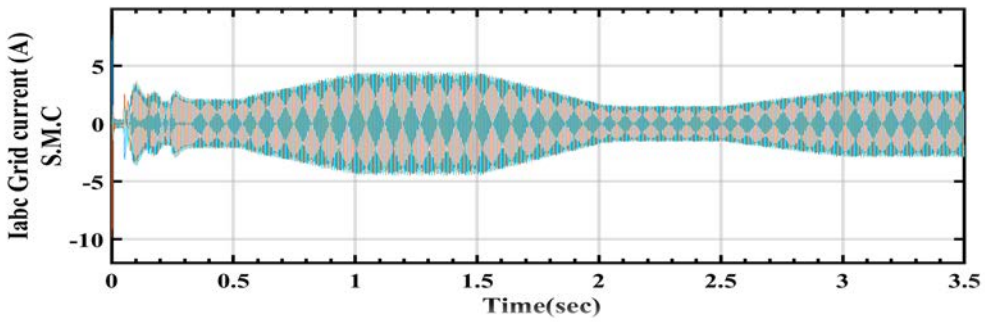

(**A**)

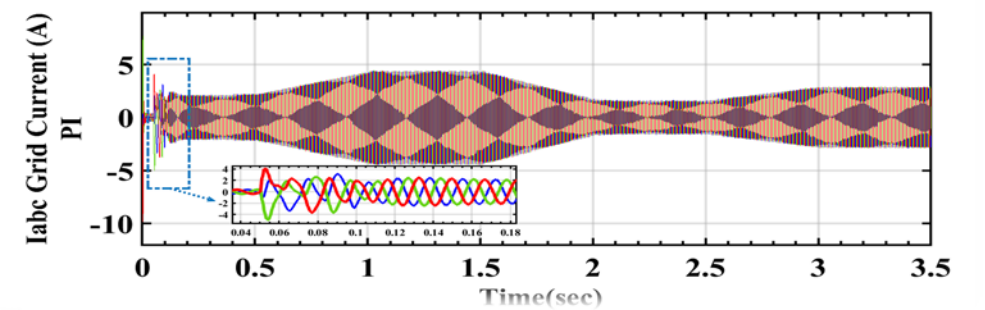

(**B**)

Figure 11. Grid current under ramp change irradiance (**A**) SMC and (**B**) PI control.

The voltage stability in the PI control and SMC systems are shown in Figure 12A and Figure 12B, respectively. It is evident that both control strategies are successful in keeping the voltage output steady. These numbers clearly show how stable the voltage output is, which supports the efficacy of the SMC and PI control systems at sustaining a steady and dependable voltage level.

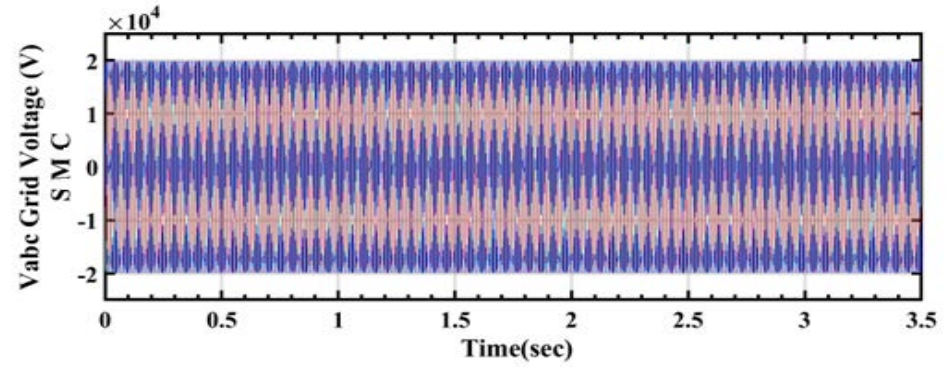

(**A**)

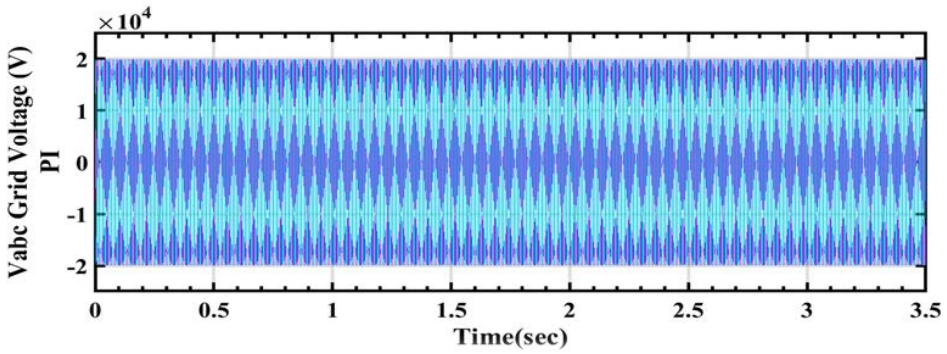

(**B**)

Figure 12. Grid voltage under ramp change irradiance (**A**) SMC and (**B**) PI control.

3.2. Comparison Results under Random Changes in Solar Radiation

A sample profile with random changes in solar radiation around an average value of 400 W/m^2 is shown in Figure 13. The ambient temperature stays constant in this profile. Things like cloud cover or wet days may cause these erratic variations in solar energy. In these difficult circumstances, addressing such unanticipated variations in radiation doses is essential to guaranteeing the efficacy of the proposed MPPT approach.

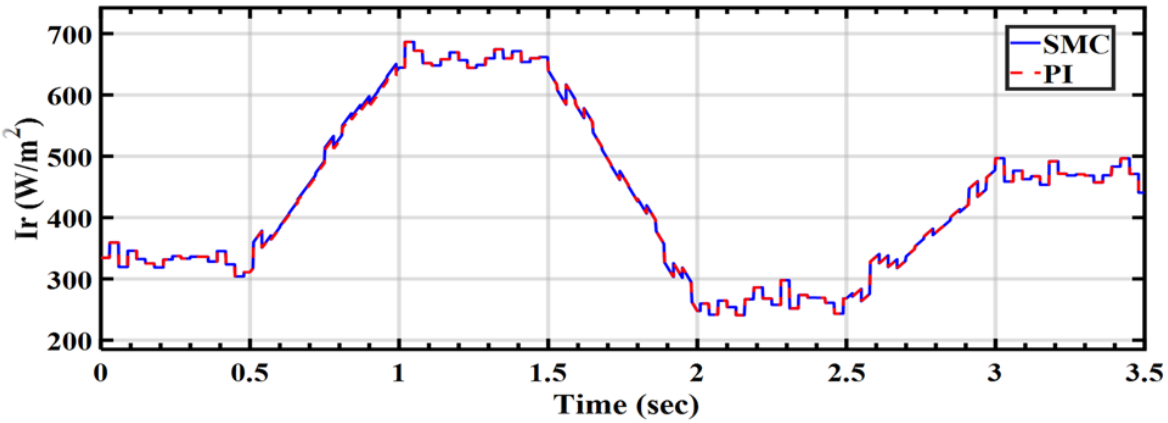

Figure 13. Irradiance in a randomly updated profile.

The PV output voltage is displayed in Figure 14A for the two distinct control systems, PI and SMC. The curve makes it clear that the SMC system performs better regarding voltage output than the traditional PI control method. Especially at high temperatures, the voltage output of the SMC system is higher and more stable than that of the traditional PI control system. Furthermore, as the curve shows, the system responds more quickly under SMC than it does under PI control. Thus, in terms of voltage stability and response time, SMC can be regarded as a superior control technique for PV systems.

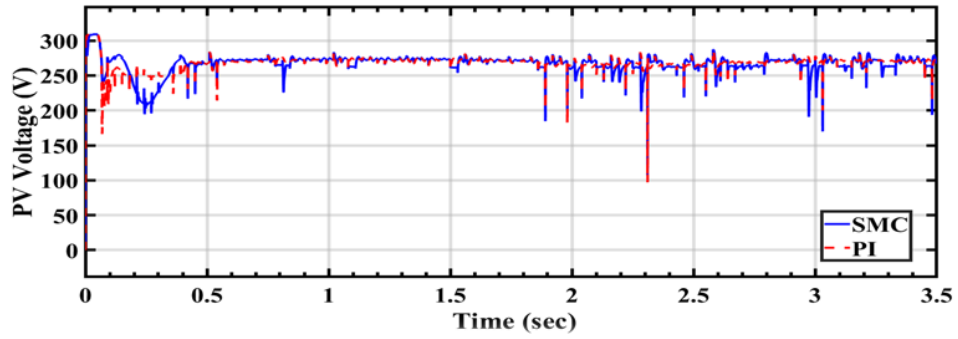

(**A**)

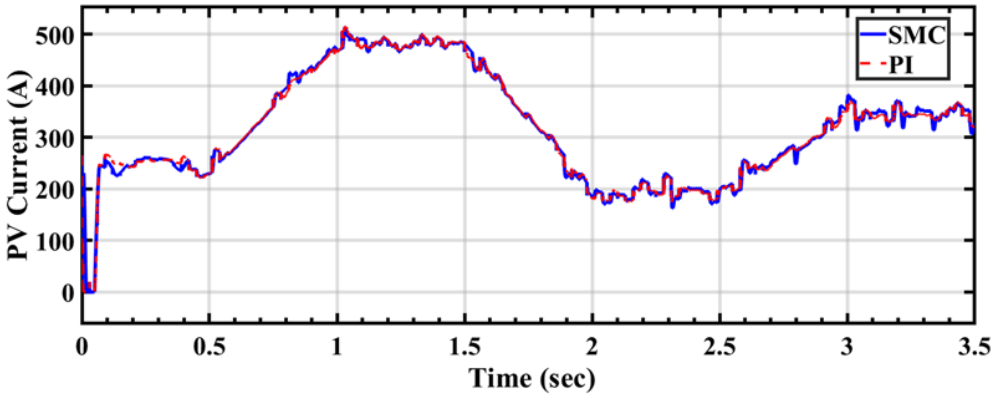

(**B**)

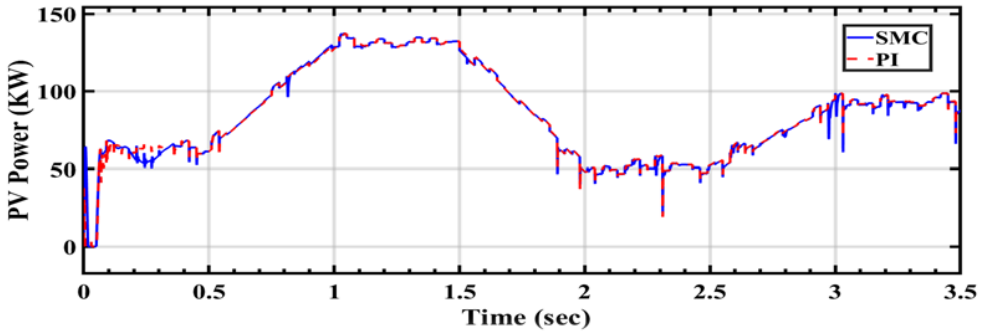

(**C**)

Figure 14. (**A**) PV voltage, (**B**) PV current, and (**C**) PV power.

Furthermore, the suggested SMC method shows better tracking of the maximum PV current than the PI control system, when comparing the PV system's current production under random variations in solar radiation, as shown in Figure 14B. In order to maximize energy output in PV systems, it is imperative that the maximum PV current be extracted more quickly and accurately, which is ensured by this improved tracking capacity. Further-

more, with quick random fluctuations in solar radiation, the PV output power in the SMC approach performs better than that of the PI control method, as illustrated in Figure 14C. Lastly, it is clear that the SMC system continuously performs better than the PI control system when comparing the performance of the standard SMC and PI control systems under quickly changing weather circumstances that affect solar radiation.

Figure 15 shows that the d-axis component of the active current changes from −1 PU to 1 PU, whereas the q-axis component of the reactive current stays at zero. The PV system's current response to sporadic variations in solar radiation for both the PI control and SMC systems is depicted in the figure. Both control systems' d-axis currents track variations in solar radiation rather well, although the SMC system is less oscillatory and more precisely monitors the maximum current than the PI control system. As expected from a grid-connected PV system without a reactive power injection, the q-axis current for both control systems stays at zero. As seen in Figure 16, the active power (P) reacts to spontaneous variations in solar radiation. The P of the SMC system is higher in energy output, indicating that this control system utilizes PV more effectively. A similar response is observed in the PI system, as indicated by its curve.

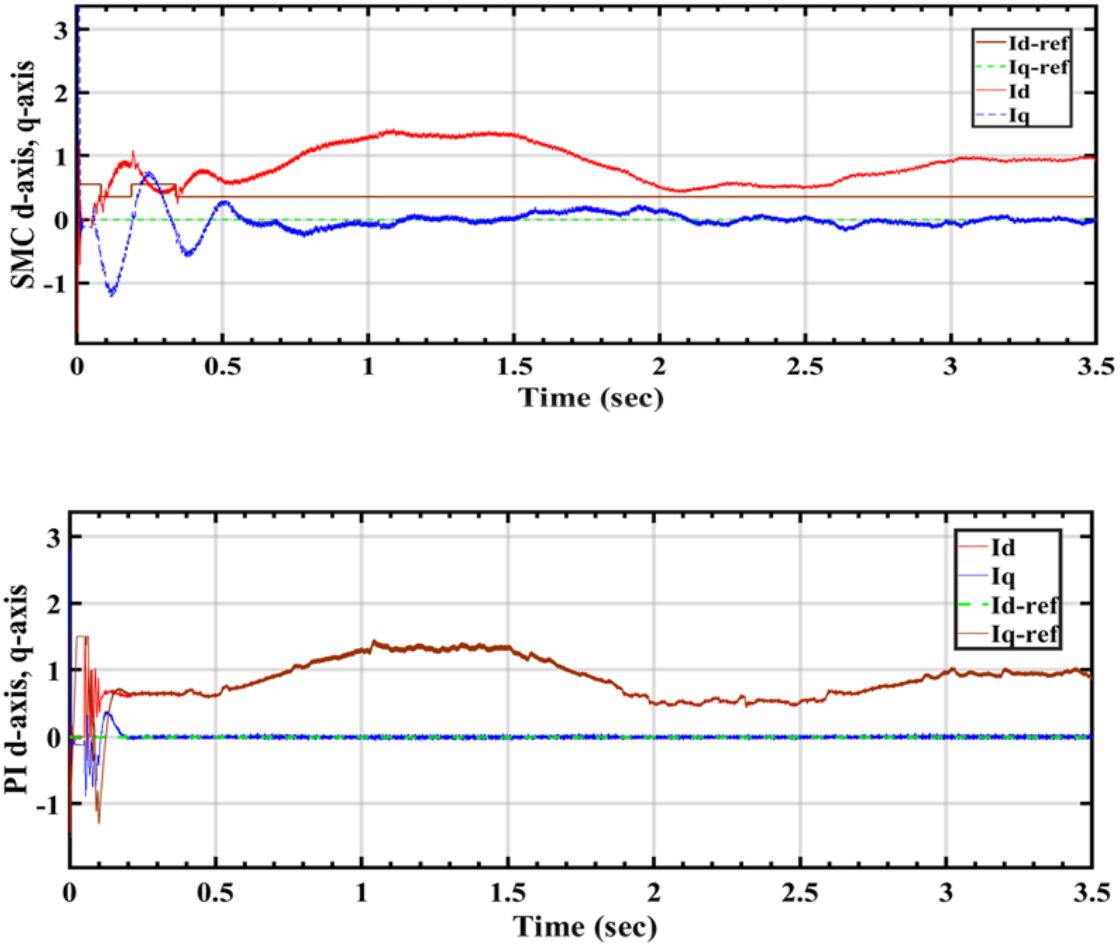

Figure 15. d-axis and q-axis currents under random change irradiance.

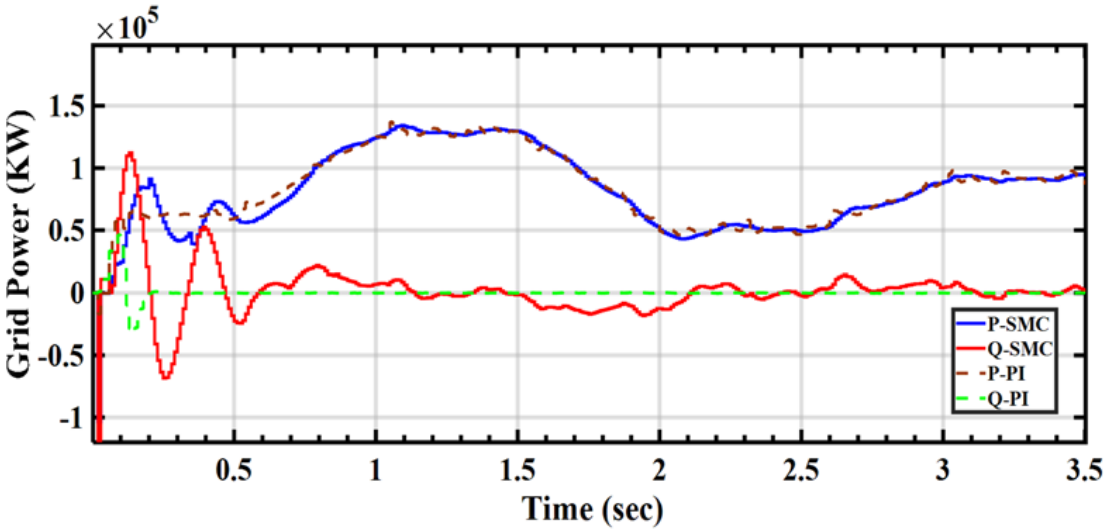

Figure 16. Grid active and reactive power under random change irradiance.

The control system can provide grid voltage stability, as seen in Figure 17, where the Vd values for the PI and SMC systems are both near to 1PU. Furthermore, both systems attain remarkable efficiency, as seen by Vq values that are nearly zero, which suggests that the reactive power is tightly managed. The ability of the PI control and SMC systems to sustain grid voltage stability is used to assess their performance (Figure 17). The grid voltage's d- and q-axes components' values over time are displayed in the figure (Vd, Vq, respectively). Grid voltage stability can be achieved by both the SMC and PI control systems, with Vd values for each system being very near to 1 per unit (PU). This indicates that the grid's voltage level is tightly managed and kept in close proximity to the reference value. Furthermore, both systems' Vq values are very near to zero, suggesting that the reactive power is under good control. Reactive power is a significant part of power flow in a power system, and stable and effective system operation depends on its effective control. As a result, attaining high efficiency and effective reactive power management is crucial for any power control system's performance assessment.

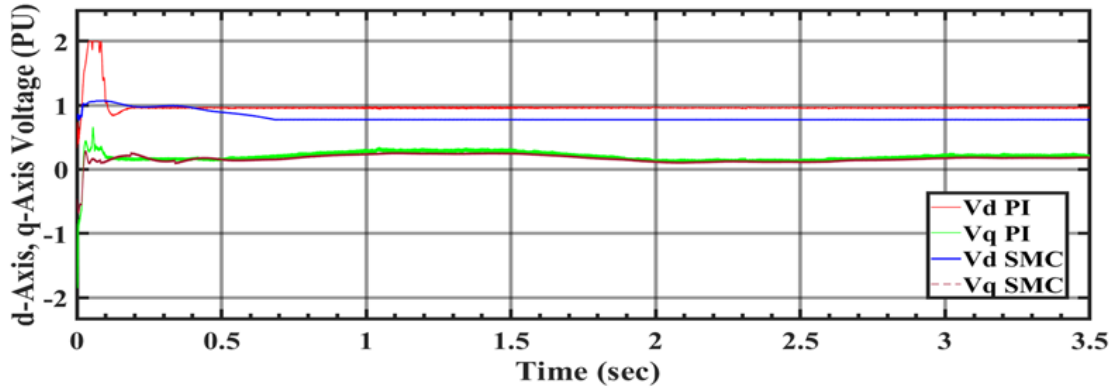

Figure 17. d-axis and q-axis voltage (PU).

The performance comparison of a PV energy system under PI and SMC with random changes in solar radiation is shown in Table 5. It shows the data for different time intervals and sun irradiance levels. The power output (PPV) and voltage output (VPV) fluctuate under the PI control over different solar irradiation levels and time intervals. For example, for the time interval of 0 to 0.5 s, the voltage varies between 209.678 V and 254.322 V, resulting in power outputs of 60.5241 kW and 54.667 kW, with an irradiance range of

331.324 to 360.025 W/m^2. A greater output voltage and power stability over the same irradiance levels and periods are shown with the SMC. For instance, for the mentioned irradiance range and time interval, the voltage remains relatively stable, at approximately 254.253 V and 274.682 V, with power outputs of 67.995 kW and 68.0101 kW, respectively.

Table 5. Comparison of PV energy performance for PI and SMC under random changes in solar radiation.

Type of Controller	Irradiance (W/m^2)	Time (s)	V_{PV} (V)	P_{PV} (KW)
PI	331.324:360.025	0:0.5	209.678 (fluctuations)	60.5241
			254.322 (fluctuations)	54.667
	686.285:659.676	1:1.5	272.955 (fluctuations)	129.118
			264.094 (fluctuations)	131.837
	247.793:297.868	2:2.5	230.094 (fluctuations)	22.0368
			225.002 (fluctuations)	41.2277
SMC	331.324:360.025	0:0.5	254.253	67.995
			274.682	68.0101
	686.285:659.676	1:1.5	279.641	136.442
			275.551	134.224
	247.793:297.868	2:2.5	270.235	58.4029
			271.341	50.9526

Figure 18 represents the relationship between the modulation index and inverter output for the SMC and PI control systems. The modulation index is the ratio of the modulating signal's peak amplitude to the carrier signal's peak amplitude. The modulation index is important for determining the inverter output voltage and current harmonics. The x-axis shows the modulation index, while the inverter output is represented by the y-axis. The blue curve shows the inverter output for the SMC system, and the red curve represents the PI control system's inverter output. The maximum modulation index is one, beyond which the system becomes unstable, and the inverter output becomes distorted. Both curves show that the inverter output increases with an increasing modulation index until a maximum value is reached. Beyond the maximum value, the output becomes distorted, which indicates that the inverter is operating beyond its limits.

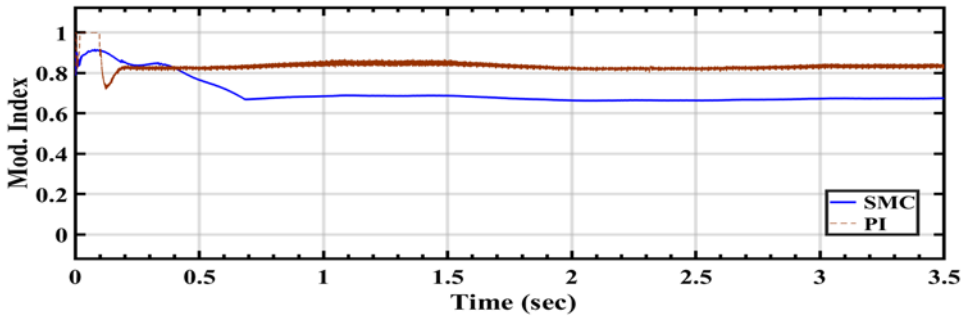

Figure 18. Modulation index.

The modulation index must be kept below the upper limit to guarantee system stability and lessen harmonics in the inverter output. As seen in Figure 18, both control systems can control the inverter output within the stable region, but because of its quick and reliable control mechanism, the SMC system produces a more accurate output.

The grid performance of the PI and SMC under random changes in solar radiation are compared in Table 6. The table shows the grid power output (W), grid current in the d-axis (Grid Id), and grid current in the q-axis (Grid Iq), with each row denoting a certain time interval. When under the PI control, the grid power output and currents fluctuate across the different time intervals. At 0.1313 s, for instance, the grid power output is recorded as 65.361 kW, and the related Grid Id and Grid Iq are 0.6566 and 0.3304, respectively. The SMC, on the other hand, shows a more reliable grid performance over the same time intervals. The Grid Id and Grid Iq are 0.7512 and −1.111, respectively, when the grid power output stabilizes at 77.872 kW at 0.1313 s. Comparing the SMC to PI control amid random fluctuations in solar radiation, these results demonstrate the SMC's capacity to maintain consistent grid functioning. The SMC's more dependable management of grid power output and currents suggests potential gains in grid stability and reliability.

Table 6. Comparison of grid performance results for PI and SMC under random changes in solar radiation.

Type of Controller	Time (s)	Grid Power (kW)	Grid I_d	Grid I_q
PI	0.1313	65.361.1	0.6566	0.3304
	0.6805	61.208	0.7927	0.0024
	1.2514	131.599	1.2703	0.0101
	2.1982	49.096	0.5432	0.0257
	2.5216	46.655	0.5187	0.0131
	3.2151	91.754	0.9514	0.0362
SMC	0.1313	77.872	0.7512	1.111-
	0.6805	71.235	0.6127	0.0061-
	1.2514	128.404	1.3275	0.0503-
	2.1982	54.246	0.5045	0.05644
	2.5216	49.933	0.4676	0.05244
	3.2151	91.941	0.9231	0.04241

Figure 19 shows how three-phase currents in a PV system relate to one another when solar radiation varies. The time is shown on the x-axis, and the current values are shown on the y-axis. The dotted line represents the b- and c-phase currents, while the solid line represents the a-phase current. Figure 19 illustrates how variations in solar energy cause corresponding variations in current, allowing the system to track the MPPT efficiently. The MPPT indicates the maximum power output point on the PV panel's current–voltage curve. It essentially represents the circumstances in which the PV panel produces the maximum amount of power. The current relationships under the various control methods are depicted in Figure 19. The current relationship under the SMC system is shown in Figure 19A, while the current relationship under the PI control system is shown in Figure 19B. The two control systems are able to track the MPPT, and their present levels are nearly in sync. On the other hand, the SMC system responds faster and tracks the MPPT more accurately than the PI control system.

The output voltage of a PV system is shown in Figure 20A,B for two distinct control schemes: SMC and PI control. An essential component of a PV system is voltage stability, which depends on maintaining a steady voltage level to guarantee effective energy use. Figure 20 shows that both control strategies can keep the voltage level constant, demonstrating how well they can regulate a PV system. On the other hand, the voltage output of the SMC system seems to be a little bit smoother than that of the PI control system. This is extremely important, because voltage stability directly affects a PV system's power output. At the MPPT, when the power output is optimized, the system can function with stable voltage levels. For effective energy generation, it is therefore essential to maintain a steady voltage output in both control schemes.

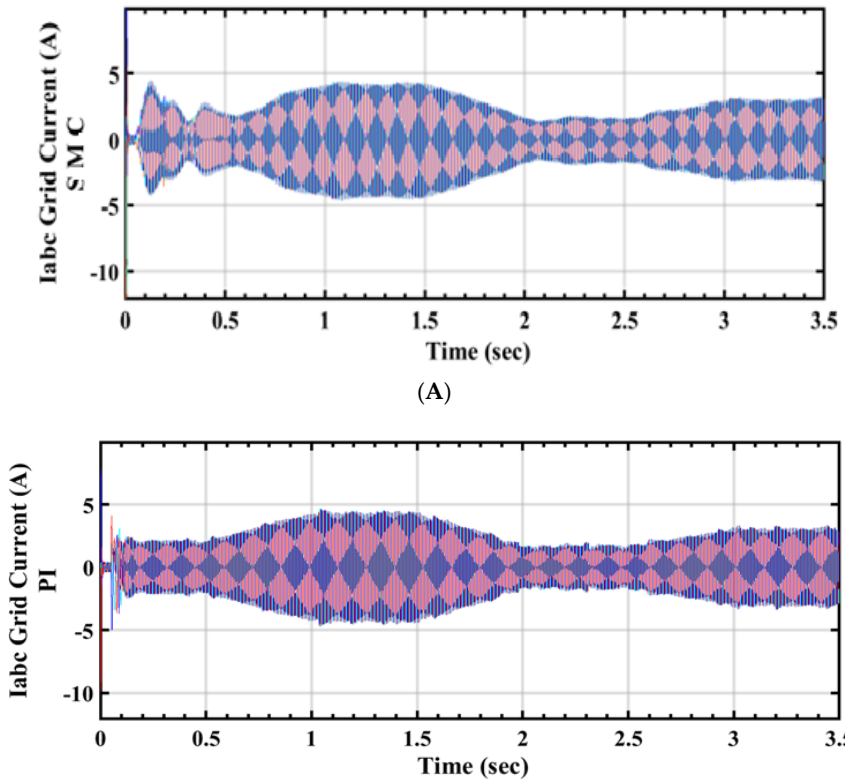

Figure 19. Grid current under random change irradiance (**A**) SMC and (**B**) PI control.

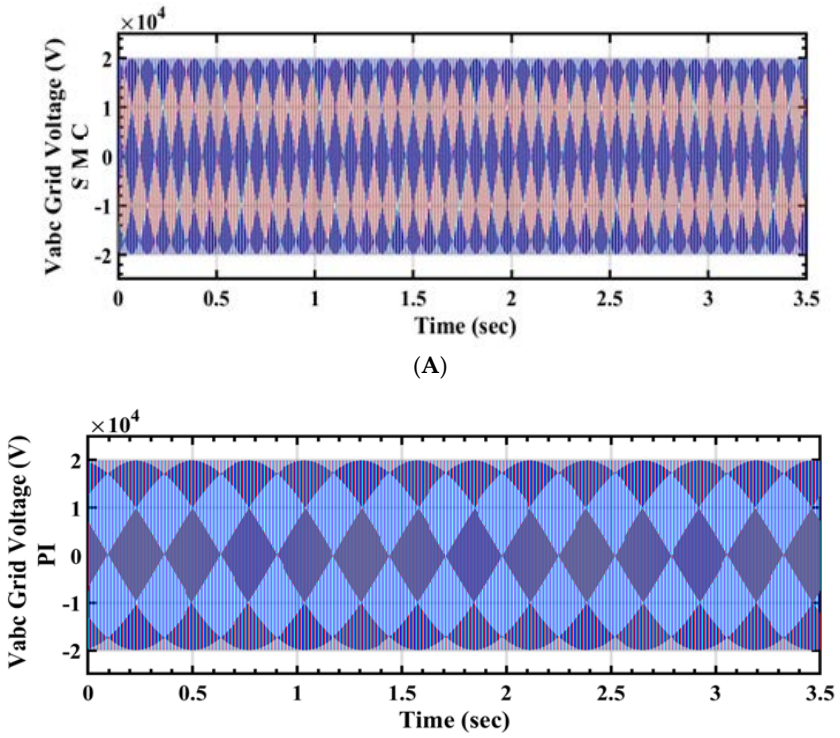

Figure 20. Grid voltage under random change irradiance (**A**) SMC and (**B**) PI control.

4. Conclusions

In conclusion, the research described in this work focused on comparing and implementing PI control and SMC schemes, two different control methods. Improving a PV system's performance was the main goal. The results demonstrate the greater effectiveness of the SMC system over the PI control system in a number of critical areas, such as precision, efficiency, and stability. In particular, the PV system's maximum power point was tracked with remarkable accuracy by the SMC system, even in difficult conditions with rapid and unpredictable variations in solar radiation brought on by weather patterns. This performance stands in sharp contrast to that of the PI control system, which showed reduced precision and stability and increased oscillations in the active current. The SMC system also showed excellent grid voltage and current stability.

Additionally, it improved the modulation index relationship, which is a key component for controlling power electronic systems' control dynamics. Compared to the PI control, the SMC showed improved efficiency and stability for both voltage and power output. The power output improvements ranged from 5% to 10%, while voltage variations were reduced by almost 75%. Additionally, compared to PI management, SMC minimized grid current fluctuations by around 30% and reduced grid power output changes by about 20%, to ensure a more consistent grid performance. This study provides compelling evidence that the SMC system is a viable option for optimizing PV system performance and achieving increased energy production efficiency. Through the efficient resolution of issues concerning accuracy, stability, and power output optimization, the SMC technique has great potential to further the development of renewable energy systems. The proposed SMC has proven to be highly efficient during random radiation and, therefore, the proposed system can work effectively in a partial shading scenario.

Author Contributions: Conceptualization, H.A., S.H.H., S.A.M.A., W.S.E.A., H.Y.H., W.I.M. and M.M.; methodology, H.A., S.H.H., S.A.M.A., W.S.E.A., H.Y.H., W.I.M. and M.M.; software, H.A., S.H.H., S.A.M.A., W.S.E.A., H.Y.H., W.I.M. and M.M.; validation, H.A., S.H.H., S.A.M.A., W.S.E.A., H.Y.H., W.I.M. and M.M.; formal analysis, H.A., S.H.H., S.A.M.A., W.S.E.A., H.Y.H., W.I.M. and M.M.; investigation, H.A., S.H.H., S.A.M.A., W.S.E.A., H.Y.H., W.I.M. and M.M.; resources, H.A., S.H.H., S.A.M.A., W.S.E.A., H.Y.H., W.I.M. and M.M.; data curation, H.A., S.H.H., S.A.M.A., W.S.E.A., H.Y.H., W.I.M., M.M., H.A., S.H.H., S.A.M.A., W.S.E.A., H.Y.H., W.I.M. and M.M.; writing—review and editing, H.A., S.H.H., S.A.M.A., W.S.E.A., H.Y.H., W.I.M. and M.M.; visualization, H.A., S.H.H., S.A.M.A., W.S.E.A., H.Y.H., W.I.M. and M.M.; funding acquisition, H.A. and S.H.H. All authors have read and agreed to the published version of the manuscript.

Funding: This research was funded by Research & Innovation, Ministry of Education in Saudi Arabia for funding this research work through the project number ISP-2024.

Institutional Review Board Statement: Not applicable.

Informed Consent Statement: Not applicable.

Data Availability Statement: The data presented in this study are available on request from the corresponding authors.

Acknowledgments: The authors extend their appreciation to the Deputyship for Research & Innovation, Ministry of Education in Saudi Arabia for funding this research work through the project number ISP-2024.

Conflicts of Interest: The authors declare no conflicts of interest.

References

1. Saleh, B.; Yousef, A.M.; Abo-Elyousr, F.K.; Mohamed, M.; Abdelwahab, S.A.M.; Elnozahy, A. Performance Analysis of Maximum Power Point Tracking for Two Techniques with Direct Control of Photovoltaic Grid-Connected Systems. *Energy Sources Part A Recovery Util. Environ. Eff.* **2021**, *44*, 413–434. [CrossRef]
2. Rekioua, D.; Bensmail, S.; Bettar, N. Development of hybrid photovoltaic-fuel cell system for stand-alone application. *Int. J. Hydrog. Energy* **2013**, *39*, 1604–1611. [CrossRef]

3. Hwang, J.J.; Lai, L.K.; Wu, W.; Chang, W.R. Dynamic modeling of a photovoltaic hydrogen fuel cell hybrid system. *Int. J. Hydrog. Energy* **2009**, *34*, 9531–9542. [CrossRef]
4. Yunez-Cano, A.; González-Huerta, R.G.; Tufiño-Velázquez, M.; Barbosa, R.; Escobar, B. Solar-hydrogen hybrid system integrated to a sustainable house in Mexico. *Int. J. Hydrog. Energy* **2016**, *41*, 19539–19545. [CrossRef]
5. Yousef, A.M.; Ebeed, M.; Abo-Elyousr, F.K.; Elnozohy, A.; Mohamed, M.; Abdelwahab, S.A.M. Optimization of PID Controller for Hybrid Renewable Energy System Using Adaptive Sine Cosine Algorithm. *Int. J. Renew. Energy Res.-IJRER* **2020**, *10*, 670–677.
6. Xu, X.; Li, Y.; Yan, Z.; Ma, H.; Shahidehpour, M. Hierarchical Central-Local Inverter-Based Voltage Control in Distribution Networks Considering Stochastic PV Power Admissible Range. *IEEE Trans. Smart Grid* **2023**, *14*, 1868–1879. [CrossRef]
7. Gulzar, M.M.; Iqbal, A.; Sibtain, D.; Khalid, M. An Innovative Converterless Solar PV Control Strategy for a Grid Connected Hybrid PV/Wind/Fuel-Cell System Coupled with Battery Energy Storage. *IEEE Accesss* **2023**, *11*, 23245–23259. [CrossRef]
8. Wang, H.; Hua, L.; Guo, Y.; Lu, C. Control of Z-Axis MEMS Gyroscope Using Adaptive Fractional Order Dynamic Sliding Mode Approach. *IEEE Access* **2019**, *7*, 133008–133016. [CrossRef]
9. Ibrahim, N.F.; Mahmoud, K.; Lehtonen, M.; Darwish, M.M.F. Comparative Analysis of Three-Phase PV Grid Connected Inverter Current Control Schemes in Unbalanced Grid Conditions. *IEEE Access* **2023**, *11*, 42204–42221. [CrossRef]
10. Mishra, M.K.; Lal, V.N. A Multiobjective Control Strategy for Harmonic Current Mitigation with Enhanced LVRT Operation of a Grid-Tied PV System without PLL Under Abnormal Grid Conditions. *IEEE J. Emerg. Sel. Top. Power Electron.* **2023**, *11*, 2164–2177. [CrossRef]
11. Sonawane, A.J.; Umarikar, A.C. Voltage and Reactive Power Regulation with Synchronverter-Based Control of PV-STATCOM. *IEEE Access* **2023**, *11*, 52129–52140. [CrossRef]
12. Gao, P.; Zhang, G.; Ouyang, H.; Mei, L. An Adaptive Super Twisting Nonlinear Fractional Order PID Sliding Mode Control of Permanent Magnet Synchronous Motor Speed Regulation System Based on Extended State Observer. *IEEE Access* **2020**, *8*, 53498–53510. [CrossRef]
13. Xu, S.S.; Chen, C.; Wu, Z. Study of Nonsingular Fast Terminal Sliding-Mode Fault-Tolerant Control. *IEEE Trans. Ind. Electron.* **2015**, *62*, 3906–3913. [CrossRef]
14. Zhang, X.; Zhou, Z. Integrated fault estimation and fault tolerant attitude control for rigid spacecraft with multiple actuator faults and saturation. *IET Control Theory Appl.* **2019**, *13*, 2365–2375. [CrossRef]
15. Khorashadi-Zadeh, H. Power transformer differential protection scheme based on symmetrical component and artificial neural network. In Proceedings of the 7th Seminar on Neural Network Applications in Electrical Engineering, 2004 NEUREL, Belgrade, Serbia, 23–25 September 2004; pp. 261–265.
16. Mishra, S.; Ramasubramanian, D.; Sekhar, P.C. A Seamless Control Methodology for a Grid Connected and Isolated PV-Diesel Microgrid. *IEEE Trans. Power Syst.* **2013**, *28*, 4393–4404. [CrossRef]
17. Abdelwahab, S.A.M.; Hegazy, H.Y.; Mohamed, W.I. Experimental investigation and theoretical for the performance improvement of MPPT technique with PV systems connected to the grid. *Int. J. Smart Grid Clean Energy* **2021**, *10*, 253–269. [CrossRef]
18. Moustafa, G.; Ginidi, A.R.; Elshahed, M.; Shaheen, A.M. Economic environmental operation in bulk AC/DC hybrid interconnected systems via enhanced artificial hummingbird optimizer. *Electr. Power Syst. Res.* **2023**, *222*, 109503. [CrossRef]
19. Smaili, H.; Almalawi, D.R.; Shaheen, A.M.; Mansour, H.S.E. Optimizing PV Sources and Shunt Capacitors for Energy Efficiency Improvement in Distribution Systems Using Subtraction-Average Algorithm. *Mathematics* **2024**, *12*, 625. [CrossRef]
20. Moustafa, G.; Smaili, I.H.; Almalawi, D.R.; Ginidi, A.R.; Shaheen, A.M.; Elshahed, M.; Mansour, H.S. Dwarf Mongoose Optimizer for Optimal Modeling of Solar PV Systems and Parameter Extraction. *Electronics* **2023**, *12*, 4990. [CrossRef]
21. Chen, J.; Park, J.H.; Xu, S. Stability Analysis for Neural Networks with Time-Varying Delay via Improved Techniques. *IEEE Trans. Cybern.* **2019**, *49*, 4495–4500. [CrossRef]
22. Yousef, A.M.; Ibrahem, H.A.; Abo-elyousr, F.K.; Mohamed, M. Sliding Mode Control for Three Phase PV Grid Connected Energy System Using LCL Filter. *Minia J. Eng. Technol.* **2017**, *36*, 10159–10174.
23. Hamed, S.B.; Abid, A.; Hamed, M.B.; Sbita, L.; Bajaj, M.; Ghoneim, S.S.M.; Zawbaa, H.M.; Kamel, S. A robust MPPT approach based on first-order sliding mode for triple-junction photovoltaic power system supplying electric vehicle. *Energy Rep.* **2023**, *9*, 4275–4297. [CrossRef]
24. Lubbad, M.M.; El-Amary, N.H.; Abdelaziz, A.Y. Sliding Mode Control for Hybrid Power Sources Micro-grid. In Proceedings of the 2019 21st International Middle East Power Systems Conference (MEPCON), Cairo, Egypt, 17–19 December 2019; pp. 650–655.
25. Qi, G.; Chen, A.; Chen, J. Improved control strategy of interlinking converters with synchronous generator characteristic in islanded hybrid AC/DC microgrid. *in CPSS Trans. Power Electron. Appl.* **2017**, *2*, 149–158. [CrossRef]
26. Elnozahy, A.; Yousef, A.M.; Abo-Elyousr, F.K.; Mohamed, M.; Abdelwahab, S.A. Performance improvement of hybrid renewable energy sources connected to the grid using artificial neural network and sliding mode control. *J. Power Electron.* **2021**, *21*, 1166–1179. [CrossRef]
27. Rmili, L.; Hamouda, M.; Rahmani, S.; Fortin, H.; Al-Haddad, B.K. PWM-based Integral Sliding-mode Controller for Unity Input Power Factor Operation of Indirect Matrix Converter. *J. Power Electron.* **2017**, *17*, 1048–1057.
28. Lin, X.; Wen, Y.; Yu, R.; Yu, J.; Wen, H. Improved Weak Grids Synchronization Unit for Passivity Enhancement of Grid-Connected Inverter. *IEEE J. Emerg. Sel. Top. Power Electron.* **2022**, *10*, 7084–7097. [CrossRef]
29. Liu, S.; Liu, C. Virtual-Vector-Based Robust Predictive Current Control for Dual Three-Phase PMSM. *IEEE Trans. Ind. Electron.* **2021**, *68*, 2048–2058. [CrossRef]

30. Taghieh, A.; Mohammadzadeh, A.; Zhang, C.; Kausar, N.; Castillo, O. A type-3 fuzzy control for current sharing and voltage balancing in microgrids. *Appl. Soft Comput.* **2022**, *129*, 109636. [CrossRef]
31. Abid, S.; El-Rifaie, A.M.; Elshahed, M.; Ginidi, A.R.; Shaheen, A.M.; Moustafa, G.; Tolba, M.A. Development of Slime Mold Optimizer with Application for Tuning Cascaded PD-PI Controller to Enhance Frequency Stability in Power Systems. *Mathematics* **2023**, *11*, 1796. [CrossRef]
32. Eker, I. Second-order sliding mode control with experimental application. *ISA Trans.* **2010**, *49*, 394–405. [CrossRef]
33. Edwards, C.; Spurgeon, S.K. *Sliding Mode Control: Theory and Applications*; Taylor & Francis: London, UK, 1998.
34. Holkar, K.S.; Waghmare, L.M. Sliding Mode Control with Predictive PID Sliding Surface for Improved Performance. *Int. J. Comput. Appl.* **2013**, *78*, 1–5.
35. Eker, I. Sliding mode control with PID sliding surface and experimental application to electromechanical plant. *ISA Trans.* **2006**, *45*, 109–118. [CrossRef] [PubMed]